ACS Photonics

pubs.acs.org/journal/apchd5

Article

Strain-Tunable Single-Photon Source Based on a Circular Bragg Grating Cavity with Embedded Quantum Dots

Magdalena Moczała-Dusanowska,*,† Łukasz Dusanowski,† Oliver Iff, Tobias Huber, Silke Kuhn, Tomasz Czyszanowski, Christian Schneider, and Sven Höfling

Cite This: https://dx.doi.org/10.1021/acsphotonics.0c01465

Read Online

ACCESS | Metrics & More | Article Recommendations | Supporting Information

ABSTRACT: We demonstrate a Purcell-enhanced single-photon source realized by the fabrication of a hybrid III−V/dielectric circular Bragg grating cavity directly bonded onto a piezoelectric actuator. Such a kind of photonic system offers the potential for broadband high photon extraction efficiency and spontaneous emission rate enhancement. This device allows for reversible spectral tuning of the embedded quantum dot emitters and pure triggered single-photon generation with $g^{(2)}(0) = (1.5 \pm 0.05) \times 10^{-3}$. By applying 18 kV/cm electric filled to the piezosubstrate, we achieve a tuning range larger than 0.78 meV for quantum dots in resonance with the cavity mode. Spontaneous emission lifetimes smaller than 200 ps, in conjunction with a systematic increase of the spontaneous emission rate on resonance with the broadband cavity mode, verify that our device operates deep in the Purcell regime. Our strain-tunable, broadband Purcell-enhanced device represents a crucial building block for scalable quantum technologies.

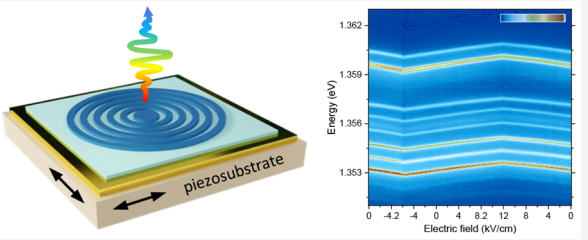

KEYWORDS: *semiconductor quantum dots, circular Bragg grating cavity, bullseye cavity, strain tuning, single-photon source*

Quantum optics technologies, such as linear optical quantum computing,[1] quantum networks,[2] or boson sampling,[3] require bright sources of indistinguishable single photons or entangled photon pairs on demand.[4] Semiconductor quantum dots (QDs) have been shown as one of the most promising photon emitters in this regard, thanks to their high quantum efficiency[5] and compatibility with mature semiconductor technology, allowing for integration with various photonic structures to increase the photon extraction efficiency.[6,7] In particular, by placing the quantum dot in a cavity, the spontaneous emission rate experiences a significant enhancement via the Purcell effect. Apart from boosting the single-photon flux, this allows reducing the impact of decoherence on the emitter and has been utilized as a tool to generate highly indistinguishable single photons.[8−10] Nearly ideal single-photon performance with over 98% indistinguishability has been recently reported for QDs coupled to micropillar cavities.[11,12] Such types of resonators are characterized by a spectrally narrow cavity mode. On the other hand, there exists a class of quantum optics applications, where a broadband cavity is on high demand. This kind of structure would allow for Purcell enhancement of multiple spectrally separated transitions in the QD, desired for entangled photon pair generation based on the exciton−biexciton cascade,[4,13] photonic cluster states formation,[14] or spin-photon entanglement.[15,16] Ideally, it ought to feature a broad operation bandwidth with maximized Purcell enhancement, which can be realized based on devices featuring a small mode volume and moderate cavity quality factor. Different types of photonic cavity structures were suggested toward this goal, including H1 photonic crystal cavities,[17] a combination of epitaxially grown distributed Bragg reflector (DBR) with a sophisticated appearance like trumpet[18] or hourglass[19] geometry and cavities consisting of a circular disk surrounded by a set of concentric rings[20,21] in the thin membrane, known in the literature as circular Bragg grating (CBG), or bullseye cavities.

Among the mentioned approaches, the CBG cavities are especially interesting due to the rather simple design, making it feasible to scale it between different emission wavelengths from 780 nm[22] through 900−950 nm,[21,23] 1300 nm up to 1550 nm while promising a photon extraction efficiency above 90% and a Purcell factor exceeding 20.[23] In general, two types of CBG cavities can be distinguished: (i) based on air-suspended membrane[20,21,24,25] and (ii) based on a membrane bonded to a metallic mirror separated by a thin dielectric layer such as SiO_2,[22,23,26] referred to in the literature as a hybrid CBG. Recently, using hybrid CBG, Purcell-enhanced entangled

Received: September 21, 2020

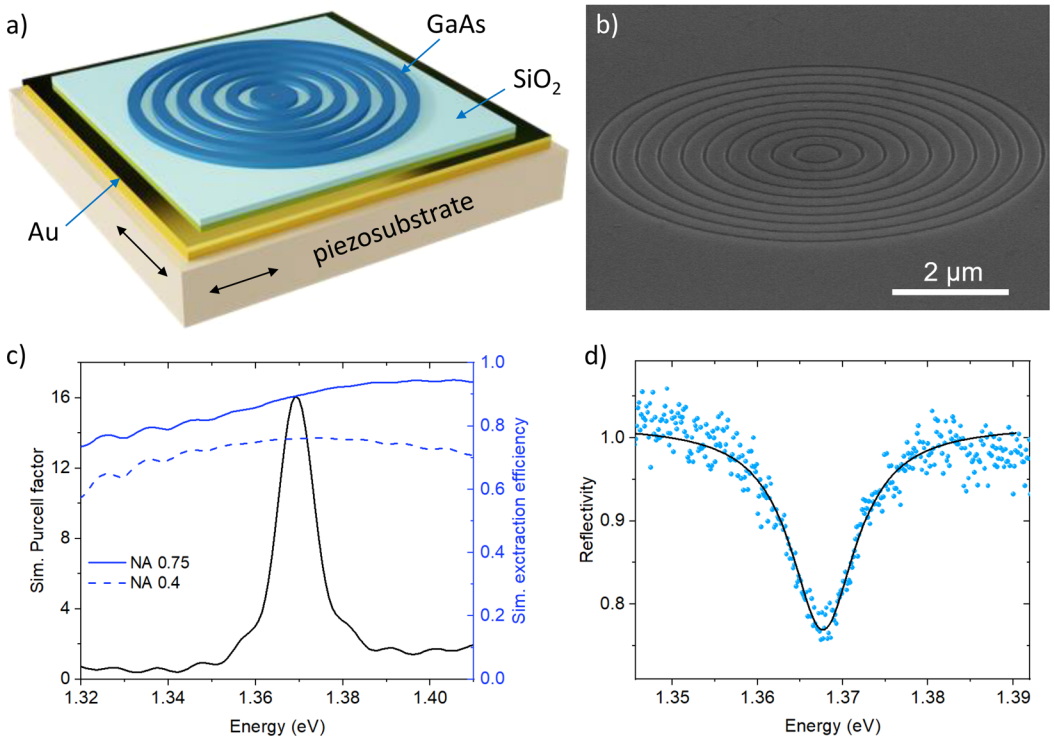

Figure 1. CBG cavity strain-tunable single-photon source. (a) An artistic sketch of the device composed of a 125 nm GaAs membrane with In(Ga)As QDs, a 360 nm layer of SiO_2, and a back reflecting gold mirror bonded to the piezosubstrate. (b) An SEM image of the fabricated device consisting of concentric rings with a central disc diameter of 760 nm. (c) Simulated Purcell factor and extraction efficiency (right axis, indicated in blue) for 0.4 and 0.75 NA collection optics as a function of energy. (d) Reflection spectra of the cavity mode with the quality factor of 146 ± 5 and fwhm of 9.34 ± 0.31 meV. The black solid line is a Lorentzian fit.

photon pairs generation with simultaneously high efficiency, fidelity, and indistinguishability was demonstrated.[22,23]

The self-assembled nature of semiconductor QDs growth results in a distribution of dots shapes, compositions, and sizes over the wafer. In order to gain control over the particular emitter energy, some postprocessing reversible spectral fine-tuning is needed. In particular, control over the emitted photon energy is essential for precise frequency matching of QDs transitions with atomic resonances or other quantum emitters. However, the easily available temperature tuning spoils the coherence of the source[27] and spectral tuning via the application of the electric fields would require the non-straightforward implementation of a p-i-n diode and electrical contacts. An alternative method for tuning quantum dots is strain tuning obtained by applying external stress generated by a piezosubstrate[28,29] which has been proved to not corrupt the indistinguishability of the source.[30] This method has been shown as a feasible technique of manipulating the QD emission in different photonic structures, including planar DBR cavities,[31] nanowires,[32] photonic crystal cavities,[33−35] photonic circuits,[36] and most recently in micropillars,[37] deterministic microlenses,[38] and parabolic cavities.[39]

In this work, we present the successful implementation of a strain-tunable single-photon source based on the hybrid CBG cavity with embedded QDs on top of a piezoelectric actuator. Through applying biaxial stress, we can reversibly shift the emission wavelength of QDs in a range of 0.78 meV. Our device displays the broadband Purcell enhancement indicated by the shortening of the decay time and pure triggered single-photon generation with $g^{(2)}(0)$ value of $(1.5 \pm 0.05) \times 10^{-3}$.

Our device is based on epitaxially grown self-assembled In(Ga)As QDs embedded in a 125 nm thick GaAs membrane. Underneath the QD layer, a 1000 nm thick $Al_{0.8}Ga_{0.2}As$ sacrificial layer is situated. Both layers have been grown on a silicon doped GaAs wafer. On top of the GaAs membrane, a SiO_2 layer with a thickness of 360 nm has been sputtered and subsequently, a gold mirror has been evaporated. To fabricate a bullseye cavity a polymer-based resin (Cyclotene 3000) was used to bond the top sample's surface to a 250 μm thick $[Pb(Mg_{1/3}Nb_{2/3})O_3]_{0.72}[PbTiO_3]_{0.28}$ (PMN-PT) piezoelectric substrate with top and bottom chromium/gold contacts. The GaAs substrate was mechanically lapped down to a thickness of approximately 30 μm. Afterward, we removed the remaining GaAs substrate via selective wet etching in citric acid (1:1 weight ratio with deionized water)/H_2O_2 (30%) (4:1) and the $Al_{0.8}Ga_{0.2}As$ sacrificial layer by subsequent wet etching in HF (5%) solution, yielding the final layer structure of the device sketched in Figure 1a. In the next steps, high-resolution electron beam lithography and a subsequent lift-off process were used to define bullseye cavities designed by numerical simulations using Plane Wave Admittance Method[40] (see Supporting Information). The pattern was transferred to the GaAs membrane using reactive ion etching with an Ar/Cl_2 plasma. The final device was mounted onto an AlN chip carrier, providing heat transfer and electrical contacts to the piezoelectric actuator via wire bonding.

A scanning electron microscope (SEM) image showing an exemplary CBG cavity mounted on the piezosubstrate with the central disc diameter d of 760 nm is presented in Figure 1b. The fabricated CBG cavity features a small effective mode volume of $V_m = 1.3(\lambda/n)^3$ in combination with a low Q cavity.

https://dx.doi.org/10.1021/acsphotonics.0c01465
ACS Photonics XXXX, XXX, XXX−XXX

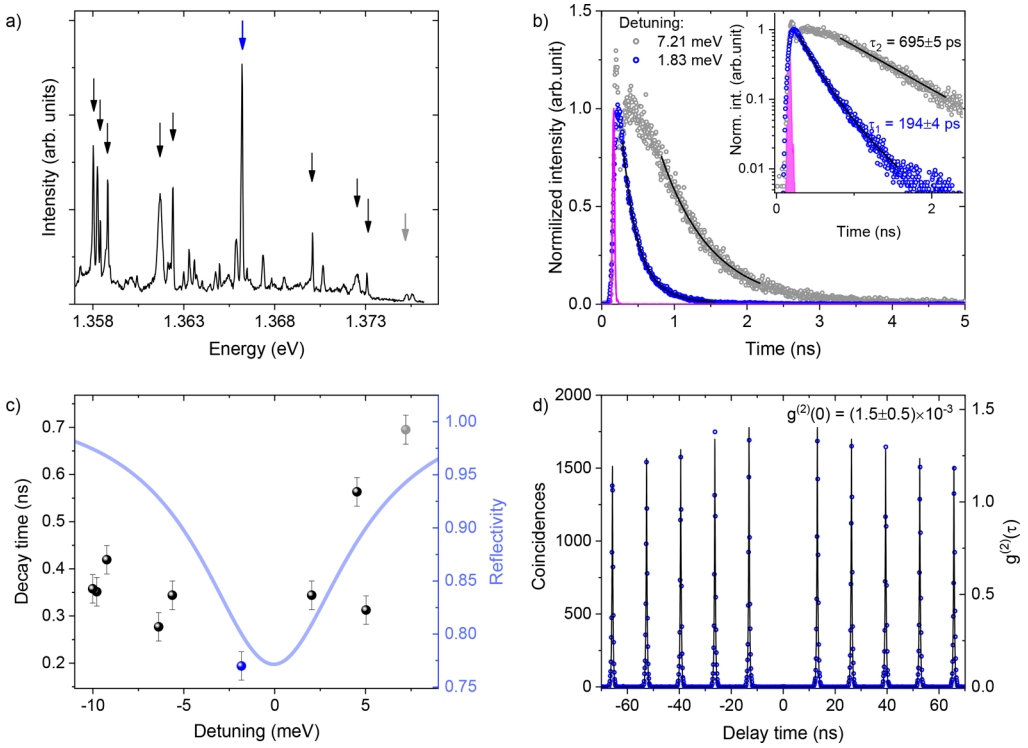

Figure 2. Optical characteristics of the strain-tunable single-photon source based on QD in the CBG cavity. (a) Photoluminescence spectrum of the bullseye device. (b) Time-resolved photoluminescence measurements. The blue and gray points are time traces recorded for the QDs emission line with energy 1.83 and 7.21 meV detuned from the cavity mode, respectively. Solid black lines indicate the exponential fits. Blue points are fitted with a biexponential function, while black points with a monoexponential function. The Signal plotted in magenta is Gaussian shape instrumental response function (IRF) with 30 ps width. Inset: Time-traces shown on a semilog scale. Please note that the spike at $t = 0$ ns on the gray data points comes from a small contribution of the scattered laser. (c) QD emission decay time vs QD-cavity-resonance detuning. Every single point corresponds to the measurement performed for a separate emission line, marked in the spectrum (a) with an arrow. The error bars correspond to a combination of fit standard deviation and IRF width. The blue solid line (right axis) is a fit of the measured reflectivity spectrum of this particular CBG device. Presented results were obtained under pulsed quasi-resonant excitation (875−885 nm) at a temperature of 4.5 K. (d) Second-order autocorrelation $g^{(2)}(\tau)$ histogram as a function of delay time between subsequently emitted photons measured under pulsed quasi-resonant excitation (902 nm) at a temperature of 4.5 K. The black solid line is an exponential decay fit taking into account emitter blinking[41] convoluted with instrumental response function (80 ps width).

For quantitative estimation of the possible Purcell enhancement and extraction efficiency, we have performed numerical simulations using finite-difference time-domain calculations. In Figure 1c, we plot the simulated Purcell factor and extraction efficiency (right axis, indicated in blue) for the collection optics with a numerical aperture (NA) of 0.4 and 0.75 as a function of the emission energy. Our simulation yields a cavity quality factor of 180, reflecting the broadband nature of the device. Remarkably, a Purcell factor as large as 16 can be theoretically obtained. Moreover, our device features about 28 meV (18 nm) bandwidth of Purcell enhancement higher than 2. Large photon extraction efficiencies above 70% (90%) can be achieved with an objective lens with NA 0.4 (0.75) maintained for about 60 meV.

The cavity mode has been characterized by the reflectivity measured at 4.5 K and is presented in Figure 1(d). The optical cavity mode peak centered at 1.368 eV energy is characterized by a full-width at half-maximum (fwhm) of 9.34 meV, corresponding to a quality factor Q of 146 ± 5 in agreement with our theoretical estimates.

The optical properties of the QDs embedded in the CBG cavities were characterized using low-temperature micro-photoluminescence (μ-PL). The μ-PL spectrum recorded for the investigated device under pulsed excitation at 882 nm wavelength is shown in Figure 2a. Several sharp peaks deriving from the emission of individual QDs are visible. To verify the possible spontaneous emission rate enhancement via the Purcell effect, we performed time-resolved photoluminescence measurements for the lines indicated with arrows. For all of them, the excitation energy was optimized individually for maximized intensity and was in the range from 1.401 to 1.417 eV (875 to 885 nm). Figure 2b depicts two exemplary μ-PL decay traces. The blue points correspond to the line positioned closest to the cavity mode with 1.83 meV detuning (indicated with the blue arrow in Figure 2a), while gray points represent the time-trace of the line detuned by 7.21 meV (indicated with the gray arrow in Figure 2a). The emission related to the 1.83 meV detuning, exhibits a much faster decay, with the characteristic time constant of τ_1 = 194 ± 4 ps, as compared to τ_2 = 695 ± 5 ps obtained for the 7.21 meV detuned line (decay time uncertainty is the exponential fit standard deviation). The instrument response function (IRF) with an fwhm of 30 ps is shown in Figure 2b (magenta line).

The characteristic photoluminescence decay times of emission lines indicated with arrows in Figure 2a as a function of QD-cavity-resonance detuning are summarized in Figure 2c. Those transitions have been characterized by polarization- and power-dependent measurements in order to exclude biexcitonic and other higher-order complex transitions, which intrinsically feature shorter decay times (see Supporting

https://dx.doi.org/10.1021/acsphotonics.0c01465
ACS Photonics XXXX, XXX, XXX−XXX

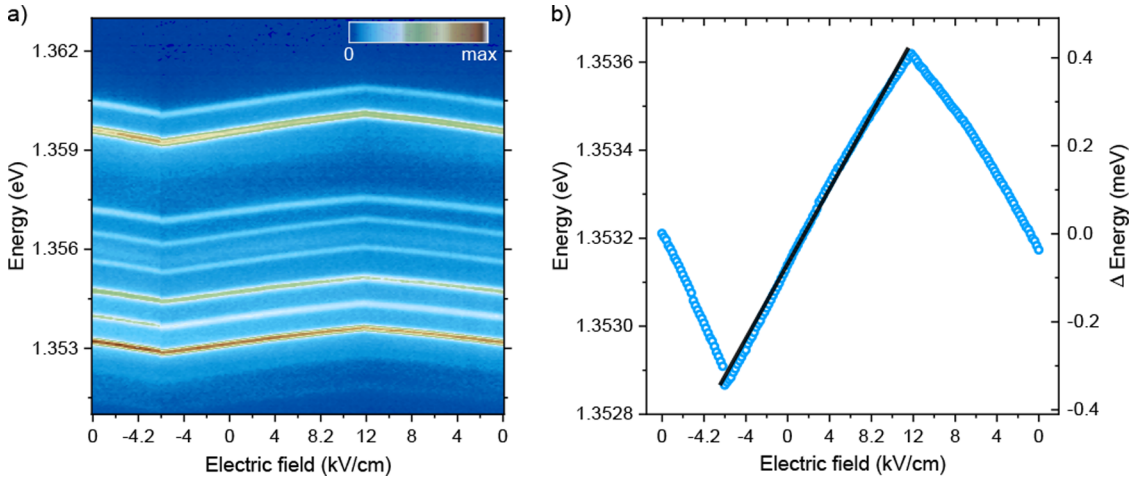

Figure 3. Strain tuning of QDs emission lines embedded in the bullseye cavity. (a) Color-coded microphotoluminescence map as a function of the applied voltage (electric field) to the piezosubstrate. (b) QD emission energy as a function of applied voltage (electric field) in the overall cycle. Blue circles show the trace of a single fitted peak of the QD emission as a function of the applied voltage. The application of external stress via the piezosubstrate induces a linear shift of the QD emission energy up to 0.78 meV for a range of 450 V applied (1.74 μeV/V).

Information). Nonmarked lines visible in the spectrum have been excluded from the analysis due to spectral wandering, weak signal-to-noise ratio, or too high background. For reference, the reflectivity spectrum of the considered CBG device has been superimposed with the blue solid line. The shortest decay times correspond to the emission lines located closest to the center of the cavity mode. With increasing detuning from the mode center, the extracted decay times increase, following the cavity spectral profile. This suggests a Purcell enhancement of emitters located within the cavity resonance. The difference in decay time constants between 695 and 194 ps suggests a spontaneous emission rate enhancement factor of around 3.5. On the other hand, the longest lifetime value (695 ps) was measured for the QD placed in the bullseye cavity with the detuning of 7.21 meV from the center of the cavity mode, and we suspect that this line is still enhanced by the cavity. Based on the calculations shown in Figure 1c, a Purcell enhancement higher than 2 is expected for emitters detuned by 14 meV from the center of the cavity mode.

For a more careful evaluation of the Purcell factor, we have examined the lifetime of QDs localized in the membrane outside of the cavity close to the bullseye device. Relying on that, we have extracted the Purcell factor based on the standard weak-coupling theoretical model, assuming that the quantum dot emission rate follows a Lorentz-like dependence as a function of detuning (see Supporting Information). Based on this analysis, we can conclude that our device supports Purcell factors in a range from 3 to 9. We note that, for the investigated device, QDs are randomly positioned within the center of the device, which might be a reason why we do not reach the Purcell factor as high as 16, predicted by the theory. This could also explain the scattering of data in the dependence of decay time in the function of detuning from cavity mode. For improved enhancement, the deterministic spatial alignment of selected QDs within the center of CBG could be potentially utilized.[22,23]

To verify the single-photon character of the investigated CBG cavity device, a second-order correlation experiment was performed. Figure 2d depicts the second-order correlation function $g^{(2)}(\tau)$ histogram of the QD emission line indicated with the blue arrow in Figure 2a under 902 nm excitation at saturation power. In this case, we utilized a cross-polarization laser rejection scheme and, after spectral filtering, observed around 15 kc/s count rate on the single-photon counting detector (before filtering 284 kc/s coupled into single-mode fiber), which corresponds to the 4.9 Mc/s total count rate collected into the first collection optics with NA = 0.4. This corresponds to the total source efficiency of around 6.5% (10.4% when taking into account QD blinking). Strong suppression of the coincidence events at zero time delay proves the generation of single photons. In order to derive the single-photon purity, we divide the integrated counts of the central peak by the mean value of the adjacent set of peaks, yielding a $g^{(2)}(0)$ value of $(1.5 \pm 0.05) \times 10^{-3}$. The presented correlation histogram exhibits blinking, which is well described by the "on−off" model from ref 41, with the τ_{on} and τ_{off} time constants of 250 and 150 ns, respectively, yielding a QD "on" state efficiency of 62.5% (see Supporting Information for more details).

Finally, the reversible piezotuneability of our device was verified. For that, μ-PL experiments were carried out in a cryostat equipped with electrical feed-through at 10 K temperature and using cw nonresonant excitation. Figure 3 depicts the QDs emission spectra tunability as a function of the voltage applied to the piezosubstrate. The PMN-PT substrate was poled in a way that a positive (negative) voltage leads to an in-plane compression (expansion) of the substrate and thus of the CBG membrane with QDs. We tune the piezo voltage between −150 and 300 V in steps of 5 V to apply biaxial strain on the QDs. Figure 3a shows a color-coded μ-PL spectral intensity map recorded for QDs located in our device as a function of the voltage (electric field) applied to the piezosubstrate. The compressive (tensile) biaxial strain results in an increase (decrease) of the QDs emission energy. All QDs emission lines follow the same trend with almost identical energy change versus applied voltage. The QD emission lines are controlled in a reversible manner, without visible degradation of the optical properties. The relation between the single fitted peak of the QD emission energy and the applied electric field to piezosubstrate is plotted in Figure 3b. We extract an overall tuning range of 0.78 meV over an electric field modification of 18 kV/cm. A linear relationship between

https://dx.doi.org/10.1021/acsphotonics.0c01465
ACS Photonics XXXX, XXX, XXX−XXX

these two parameters is clearly observed with a strain-tuning slope of 1.74 μeV/V. In our experiment, we use electric fields up to 18 kV/cm due to a limited safe voltage range of our cryostat, and the applied electric field even as large as 50 kV/cm could provide reliable reversible tuning and would increase the tuning range up to 2 meV. Moreover, the tuning range could be improved by using uniaxial stress generated by, for example, micromachined piezosubstrate.[42] Additionally, the cavity properties as a function of applied strain have been examined. We observed that our CBG bullseye cavity resonance energy and value of polarization splitting (<1 nm) are insensitive to the applied strain (see Supporting Information). To verify the influence of the applied strain on the photon emission statistics of our source we performed second-order autocorrelation experiments for various voltages applied to the piezosubstrate (see Supporting Information). No clear deterioration of the observed photon statistics was observed within the experimental error. Moreover, the influence of applied strain on the quantum dot decay time and emission line width have been studied and did not show a significant effect on them (see Supporting Information).

To conclude, we have implemented a strain-tunable single-photon source by integrating QDs embedded in the CBG cavity with piezoelectric actuator. The spontaneous emission rate enhancement of 3.5 is achieved and single-photon emission with strongly suppressed multiphoton emission events is demonstrated. Thanks to CBG capability of broadband Purcell enhancement and high extraction efficiency, tuning of QD energy could be performed without spoiling the cavity provided improved single-photon performance. This, in turn, will have profound implications for the quantum optics technologies relying on frequency matching of multiple single-photon sources. Following on that, we believe that piezotunable CBG cavity single-photon sources could find an immediate application in various quantum optics protocols, relying on multicolor driving schemes such as the generation of entangled single photon pairs, cluster states, spin-photon, and spin−spin entanglement.

■ ASSOCIATED CONTENT

Supporting Information

The Supporting Information is available free of charge at https://pubs.acs.org/doi/10.1021/acsphotonics.0c01465.

S1: Design procedure and optimization; S2: Experimental details; S3: Excitonic complexes identification; S4: Characterization of the fundamental cavity mode; S5: Purcell enhancement discussion; S6: Influence of applied strain on the single photon statistics, the QD decay time, the QD emission line width; S7: Indistinguishability of the source; S8: Blinking of the source (PDF)

■ AUTHOR INFORMATION

Corresponding Author

Magdalena Moczała-Dusanowska − *Technische Physik and Wilhelm Conrad Röntgen Research Center for Complex Material Systems, Physikalisches Institut, Würzburg University, Am Hubland 97074, Würzburg, Germany;* orcid.org/0000-0002-8023-4290; Email: magdalena.moczala@physik.uni-wuerzburg.de

Authors

Łukasz Dusanowski − *Technische Physik and Wilhelm Conrad Röntgen Research Center for Complex Material Systems, Physikalisches Institut, Würzburg University, Am Hubland 97074, Würzburg, Germany;* orcid.org/0000-0001-7543-1938

Oliver Iff − *Technische Physik and Wilhelm Conrad Röntgen Research Center for Complex Material Systems, Physikalisches Institut, Würzburg University, Am Hubland 97074, Würzburg, Germany;* orcid.org/0000-0002-3613-8605

Tobias Huber − *Technische Physik and Wilhelm Conrad Röntgen Research Center for Complex Material Systems, Physikalisches Institut, Würzburg University, Am Hubland 97074, Würzburg, Germany*

Silke Kuhn − *Technische Physik and Wilhelm Conrad Röntgen Research Center for Complex Material Systems, Physikalisches Institut, Würzburg University, Am Hubland 97074, Würzburg, Germany*

Tomasz Czyszanowski − *Photonics Group, Institute of Physics, Łódź University of Technology, 90-924 Łódź, Poland*

Christian Schneider − *Technische Physik and Wilhelm Conrad Röntgen Research Center for Complex Material Systems, Physikalisches Institut, Würzburg University, Am Hubland 97074, Würzburg, Germany; Institute of Physics, University of Oldenburg, 26129 Oldenburg, Germany*

Sven Höfling − *Technische Physik and Wilhelm Conrad Röntgen Research Center for Complex Material Systems, Physikalisches Institut, Würzburg University, Am Hubland 97074, Würzburg, Germany*

Complete contact information is available at: https://pubs.acs.org/10.1021/acsphotonics.0c01465

Author Contributions

†These authors contributed equally to this work.

Notes

The authors declare no competing financial interest.

■ ACKNOWLEDGMENTS

This work has been supported by the State of Bavaria. M.M.-D., C.S., and S.H. acknowledge funding within the QuantERA HYPER-U-P-S Project. The Project has received funding from the QuantERA ERA-NET Cofund in Quantum Technologies implemented within the European Union's Horizon 2020 Programme. T.H. and S.H. are furthermore grateful for funding by the BMBF within the Project "Q.Link.X" (FKZ: 16KIS0871). Further funding has been provided by the DFG within Project PR1749 1-1.

■ REFERENCES

(1) Barz, S. Quantum Computing with Photons: Introduction to the Circuit Model, the One-Way Quantum Computer, and the Fundamental Principles of Photonic Experiments. *J. Phys. B: At., Mol. Opt. Phys.* **2015**, *48* (8), 083001.

(2) Sangouard, N.; Simon, C.; Minář, J.; Zbinden, H.; de Riedmatten, H.; Gisin, N. Long-Distance Entanglement Distribution with Single-Photon Sources. *Phys. Rev. A: At., Mol., Opt. Phys.* **2007**, *76* (5), 050301.

(3) Wang, H.; He, Y.; Li, Y.-H.; Su, Z.-E.; Li, B.; Huang, H.-L.; Ding, X.; Chen, M.-C.; Liu, C.; Qin, J.; Li, J.-P.; He, Y.-M.; Schneider, C.; Kamp, M.; Peng, C.-Z.; Hofling, S.; Lu, C.-Y.; Pan, J.-W. High-Efficiency Multiphoton Boson Sampling. *Nat. Photonics* **2017**, *11* (6), 361−365.

(4) Akopian, N.; Lindner, N. H.; Poem, E.; Berlatzky, Y.; Avron, J.; Gershoni, D.; Gerardot, B. D.; Petroff, P. M. Entangled Photon Pairs from Semiconductor Quantum Dots. *Phys. Rev. Lett.* **2006**, *96* (13), 130501.
(5) Michler, P.; Kiraz, A.; Becher, C.; Schoenfeld, W.; Petroff, P.; Zhang, L.; Hu, E.; Imamoğlu, A. A Quantum Dot Single-Photon Turnstile Device. *Science (Washington, DC, U. S.)* **2000**, *290* (5500), 2282−2285.
(6) Michler, P. Single Semiconductor Quantum Dots. *NanoScience and Technology*; Springer, 2009; p 185, .
(7) Senellart, P.; Solomon, G.; White, A. High-Performance Semiconductor Quantum-Dot Single-Photon Sources. *Nat. Nanotechnol.* **2017**, *12* (11), 1026−1039.
(8) Santori, C.; Fattal, D.; Vučković, J.; Solomon, G. S.; Yamamoto, Y. Indistinguishable Photons from a Single-Photon Device. *Nature* **2002**, *419* (6907), 594−597.
(9) Unsleber, S.; McCutcheon, D. P. S.; Dambach, M.; Lermer, M.; Gregersen, N.; Höfling, S.; Mørk, J.; Schneider, C.; Kamp, M. Two-Photon Interference from a Quantum Dot Microcavity: Persistent Pure Dephasing and Suppression of Time Jitter. *Phys. Rev. B: Condens. Matter Mater. Phys.* **2015**, *91* (7), 075413.
(10) Grange, T.; Somaschi, N.; Antón, C.; De Santis, L.; Coppola, G.; Giesz, V.; Lemaître, A.; Sagnes, I.; Auffèves, A.; Senellart, P. Reducing Phonon-Induced Decoherence in Solid-State Single-Photon Sources with Cavity Quantum Electrodynamics. *Phys. Rev. Lett.* **2017**, *118* (25), 1−6.
(11) Somaschi, N.; Giesz, V.; De Santis, L.; Loredo, J. C.; Almeida, M. P.; Hornecker, G.; Portalupi, S. L.; Grange, T.; Antón, C.; Demory, J.; Gómez, C.; Sagnes, I.; Lanzillotti-Kimura, N. D.; Lemaítre, A.; Auffeves, A.; White, A. G.; Lanco, L.; Senellart, P. Near-Optimal Single-Photon Sources in the Solid State. *Nat. Photonics* **2016**, *10* (5), 340−345.
(12) Ding, X.; He, Y.; Duan, Z.-C.; Gregersen, N.; Chen, M.-C.; Unsleber, S.; Maier, S.; Schneider, C.; Kamp, M.; Höfling, S.; Lu, C.-Y.; Pan, J.-W. On-Demand Single Photons with High Extraction Efficiency and Near-Unity Indistinguishability from a Resonantly Driven Quantum Dot in a Micropillar. *Phys. Rev. Lett.* **2016**, *116* (2), 020401.
(13) Moreau, E.; Robert, I.; Manin, L.; Thierry-Mieg, V.; Gérard, J. M.; Abram, I. Quantum Cascade of Photons in Semiconductor Quantum Dots. *Phys. Rev. Lett.* **2001**, *87* (18), 183601.
(14) Schwartz, I.; Cogan, D.; Schmidgall, E. R.; Don, Y.; Gantz, L.; Kenneth, O.; Lindner, N. H.; Gershoni, D. Deterministic Generation of a Cluster State of Entangled Photons. *Science (Washington, DC, U. S.)* **2016**, *354* (6311), 434−437.
(15) De Greve, K.; Yu, L.; McMahon, P. L.; Pelc, J. S.; Natarajan, C. M.; Kim, N. Y.; Abe, E.; Maier, S.; Schneider, C.; Kamp, M.; Höfling, S.; Hadfield, R. H.; Forchel, A.; Fejer, M. M.; Yamamoto, Y. Quantum-Dot Spin-photon Entanglement via Frequency Down-conversion to Telecom Wavelength. *Nature* **2012**, *491* (7424), 421−425.
(16) Gao, W. B.; Fallahi, P.; Togan, E.; Miguel-Sanchez, J.; Imamoglu, A. Observation of Entanglement between a Quantum Dot Spin and a Single Photon. *Nature* **2012**, *491* (7424), 426−430.
(17) Liu, F.; Brash, A. J.; O'Hara, J.; Martins, L. M. P. P.; Phillips, C. L.; Coles, R. J.; Royall, B.; Clarke, E.; Bentham, C.; Prtljaga, N.; Itskevich, I. E.; Wilson, L. R.; Skolnick, M. S.; Fox, A. M. High Purcell Factor Generation of Indistinguishable On-Chip Single Photons. *Nat. Nanotechnol.* **2018**, *13* (9), 835−840.
(18) Gregersen, N.; McCutcheon, D. P. S.; Mørk, J.; Gérard, J.-M. J.-M.; Claudon, J. A Broadband Tapered Nanocavity for Efficient Nonclassical Light Emission. *Opt. Express* **2016**, *24* (18), 20904.
(19) Osterkryger, A. D.; Claudon, J.; Gérard, J.-M.; Gregersen, N. Photonic "Hourglass" Design for Efficient Quantum Light Emission. *Opt. Lett.* **2019**, *44* (11), 2617.
(20) Davanço, M.; Rakher, M. T.; Schuh, D.; Badolato, A.; Srinivasan, K. A Circular Dielectric Grating for Vertical Extraction of Single Quantum Dot Emission. *Appl. Phys. Lett.* **2011**, *99* (4), 041102.
(21) Sapienza, L.; Davanço, M.; Badolato, A.; Srinivasan, K. Nanoscale Optical Positioning of Single Quantum Dots for Bright and Pure Single-Photon Emission. *Nat. Commun.* **2015**, *6* (1), 7833.
(22) Liu, J.; Su, R.; Wei, Y.; Yao, B.; da Silva, S. F. C.; Yu, Y.; Iles-Smith, J.; Srinivasan, K.; Rastelli, A.; Li, J.; Wang, X. A Solid-State Source of Strongly Entangled Photon Pairs with High Brightness and Indistinguishability. *Nat. Nanotechnol.* **2019**, *14* (6), 586−593.
(23) Wang, H.; Hu, H.; Chung, T. H.; Qin, J.; Yang, X.; Li, J. P.; Liu, R. Z.; Zhong, H. S.; He, Y. M.; Ding, X.; Deng, Y. H.; Dai, Q.; Huo, Y. H.; Höfling, S.; Lu, C. Y.; Pan, J. W. On-Demand Semiconductor Source of Entangled Photons Which Simultaneously Has High Fidelity, Efficiency, and Indistinguishability. *Phys. Rev. Lett.* **2019**, *122* (11), 1−6.
(24) Ates, S.; Sapienza, L.; Davanco, M.; Badolato, A.; Srinivasan, K. Bright Single-Photon Emission From a Quantum Dot in a Circular Bragg Grating Microcavity. *IEEE J. Sel. Top. Quantum Electron.* **2012**, *18* (6), 1711−1721.
(25) Kolatschek, S.; Hepp, S.; Sartison, M.; Jetter, M.; Michler, P.; Portalupi, S. L. Deterministic Fabrication of Circular Bragg Gratings Coupled to Single Quantum Emitters via the Combination of In-Situ Optical Lithography and Electron-Beam Lithography. *J. Appl. Phys.* **2019**, *125* (4), 045701.
(26) Yao, B.; Su, R.; Wei, Y.; Liu, Z.; Zhao, T.; Liu, J. Design for Hybrid Circular Bragg Gratings for a Highly Efficient Quantum-Dot Single-Photon Source. *J. Korean Phys. Soc.* **2018**, *73* (10), 1502−1505.
(27) Muljarov, E. A.; Zimmermann, R. Dephasing in Quantum Dots: Quadratic Coupling to Acoustic Phonons. *Phys. Rev. Lett.* **2004**, *93* (23), na.
(28) Seidl, S.; Kroner, M.; Högele, A.; Karrai, K.; Warburton, R. J.; Badolato, A.; Petroff, P. M. Effect of Uniaxial Stress on Excitons in a Self-Assembled Quantum Dot. *Appl. Phys. Lett.* **2006**, *88* (20), 203113.
(29) Martín-Sánchez, J.; Trotta, R.; Mariscal, A.; Serna, R.; Piredda, G.; Stroj, S.; Edlinger, J.; Schimpf, C.; Aberl, J.; Lettner, T.; Wildmann, J.; Huang, H.; Yuan, X.; Ziss, D.; Stangl, J.; Rastelli, A. Strain-Tuning of the Optical Properties of Semiconductor Nanomaterials by Integration onto Piezoelectric Actuators. *Semicond. Sci. Technol.* **2018**, *33* (1), 013001.
(30) Reindl, M.; Jöns, K. D.; Huber, D.; Schimpf, C.; Huo, Y.; Zwiller, V.; Rastelli, A.; Trotta, R. Phonon-Assisted Two-Photon Interference from Remote Quantum Emitters. *Nano Lett.* **2017**, *17* (7), 4090−4095.
(31) Trotta, R.; Atkinson, P.; Plumhof, J. D.; Zallo, E.; Rezaev, R. O.; Kumar, S.; Baunack, S.; Schröter, J. R.; Rastelli, A.; Schmidt, O. G. Nanomembrane Quantum-Light-Emitting Diodes Integrated onto Piezoelectric Actuators. *Adv. Mater.* **2012**, *24* (20), 2668−2672.
(32) Kremer, P. E.; Dada, A. C.; Kumar, P.; Ma, Y.; Kumar, S.; Clarke, E.; Gerardot, B. D. Strain-Tunable Quantum Dot Embedded in a Nanowire Antenna. *Phys. Rev. B: Condens. Matter Mater. Phys.* **2014**, *90* (20), 201408.
(33) Luxmoore, I. J.; Ahmadi, E. D.; Luxmoore, B. J.; Wasley, N. A.; Tartakovskii, A. I.; Hugues, M.; Skolnick, M. S.; Fox, A. M. Restoring Mode Degeneracy in H1 Photonic Crystal Cavities by Uniaxial Strain Tuning. *Appl. Phys. Lett.* **2012**, *100* (12), 121116.
(34) Sun, S.; Kim, H.; Solomon, G. S.; Waks, E. Strain Tuning of a Quantum Dot Strongly Coupled to a Photonic Crystal Cavity. *Appl. Phys. Lett.* **2013**, *103* (15), 151102.
(35) Beetz, J.; Braun, T.; Schneider, C.; Höfling, S.; Kamp, M. Anisotropic Strain-Tuning of Quantum Dots inside a Photonic Crystal Cavity. *Semicond. Sci. Technol.* **2013**, *28* (12), 122002.
(36) Elshaari, A. W.; Büyüközer, E.; Zadeh, I. E.; Lettner, T.; Zhao, P.; Schöll, E.; Gyger, S.; Reimer, M. E.; Dalacu, D.; Poole, P. J.; Jöns, K. D.; Zwiller, V. Strain-Tunable Quantum Integrated Photonics. *Nano Lett.* **2018**, *18* (12), 7969.
(37) Moczała-Dusanowska, M.; Dusanowski, Ł.; Gerhardt, S.; He, Y. M.; Reindl, M.; Rastelli, A.; Trotta, R.; Gregersen, N.; Höfling, S.; Schneider, C. Strain-Tunable Single-Photon Source Based on a Quantum Dot-Micropillar System. *ACS Photonics* **2019**, *6* (8), 2025−2031.

https://dx.doi.org/10.1021/acsphotonics.0c01465
ACS Photonics XXXX, XXX, XXX−XXX

(38) Schmidt, M.; Helversen, M. v.; Fischbach, S.; Kaganskiy, A.; Schmidt, R.; Schliwa, A.; Heindel, T.; Rodt, S.; Reitzenstein, S. Deterministically Fabricated Spectrally-Tunable Quantum Dot Based Single-Photon Source. *Opt. Mater. Express* **2020**, *10* (1), 76.
(39) Lettner, T.; Zeuner, K. D.; Schöll, E.; Huang, H.; Scharmer, S.; Da Silva, S. F. C.; Gyger, S.; Schweickert, L.; Rastelli, A.; Jöns, K. D.; Zwiller, V. GaAs Quantum Dot in a Parabolic Microcavity Tuned to 87Rb D1. *ACS Photonics* **2020**, *7* (1), 29−35.
(40) Dems, M.; Kotynski, R.; Panajotov, K. Plane Wave Admittance Method - a Novel Approach for Determining the Electromagnetic Modes in Photonic Structures. *Opt. Express* **2005**, *13* (9), 3196.
(41) Santori, C.; Pelton, M.; Solomon, G.; Dale, Y.; Yamamoto, Y. Triggered Single Photons from a Quantum Dot. *Phys. Rev. Lett.* **2001**, *86* (8), 1502.
(42) Yuan, X.; Weyhausen-Brinkmann, F.; Martín-Sánchez, J.; Piredda, G.; Křápek, V.; Huo, Y.; Huang, H.; Schimpf, C.; Schmidt, O. G.; Edlinger, J.; Bester, G.; Trotta, R.; Rastelli, A. Uniaxial Stress Flips the Natural Quantization Axis of a Quantum Dot for Integrated Quantum Photonics. *Nat. Commun.* **2018**, *9* (1), 3058.

https://dx.doi.org/10.1021/acsphotonics.0c01465
ACS Photonics XXXX, XXX, XXX−XXX